Technical Physics, 2023, Vol. 68, No. 9

04

Formation of beam plasma in nitrogen atmosphere by a pulsed electron beam near a dielectric target in the forevacuum pressure range

© A.V. Kazakov,[1] E.M. Oks,[1,2] N.A. Panchenko[1]

[1] Tomsk State University of Control Systems and Radioelectronics,
634050 Tomsk, Russia
[2] Institute of High Current Electronics, Siberian Branch, Russian Academy of Sciences,
634055 Tomsk, Russia
e-mail: andrykazakov@gmail.com

Received May 18, 2023
Revised July 20, 2023
Accepted July 20, 2023

Features of the processes of beam plasma formation near a dielectric (aluminum oxide ceramic) target being irradiated by an intense pulsed electron beam in the forevacuum pressure range (4−15 Pa) have been investigated. It has been established that the density of the beam plasma near the irradiated dielectric target is higher than in the case of „free“ propagation of the electron beam. The observed increase in plasma density depends on the emission current (electron beam current), gas pressure, and accelerating voltage. The influence of the dielectric target on the beam plasma density is due to emission of electrons from the target surface and the uncompensated negative potential on the target surface, which determines the energy of emitted electrons. An increase in gas pressure leads to a smaller increase in the beam plasma density due to a decrease in the absolute value of the negative potential. Varying the electron beam current and accelerating voltage provide to control the beam plasma density.

Keywords: beam plasma, pulsed electron beam, forevacuum pressure range, plasma-cathode electron source.

DOI: 10.61011/TP.2023.09.57358.130-23

Introduction

When charged particle beams are injected and then transported through a gas medium [1–6] and when laser beams pass through a gas [7,8], the so-called beam plasma is formed. In particular, beam plasma is generated using pulsed and continuous low-energy (with energy not more than tens of keV) electron beams [4–6]. Beam plasma formed by electron beams has properties that make it an effective tool for solving various scientific and technological problems associated with plasma chemical processes [9,10], treatment (etching, activation, etc.) of the surface of materials and products [11–13], formation of protective and functional coatings [14,15], synthesis of nanoparticles [16] and a number of other applications [17,18]. Also, when using chemically active gases, the use of electron beam for plasma formation can avoid problems associated with poisoning of electrodes of conventional gas-discharge systems by products of interaction of electrode material with plasma. In addition, the electron beam method of producing beam plasma can be used to generate atomic and molecular ions, which are difficult to obtain by other methods, by evaporating a target of the desired material with an electron beam. In this case, the electron beam simultaneously provides evaporation and ionization of the target material [19].

In addition to the electron beam parameters, the density of the generated beam plasma strongly depends on the gas pressure. Therefore, forevacuum plasma electron sources [20–22], whose operating pressure (1−100 Pa) is 1−3 orders higher than for „conventional“ electron beam sources, provide the formation of a denser beam plasma. This allows effective treatment of various dielectric materials (ceramics, polymers, glass) with electron beams in the forevacuum pressure range due to the fact that the flow of positive ions from the beam plasma provides compensation for the negative charge brought by the electron beam to the surface of a nonconducting material [23,24].

Beam plasma generation in the forevacuum pressure range and its influence on the steady-state potential of a dielectric target are well enough studied for continuous electron beams with currents up to hundreds of mA [25–27]. At these currents, the negative potential is typically less than hundreds of volts and decreases as the gas pressure increases. When irradiated by an intense pulsed electron beam with high currents, the negative potential also decreases with increasing pressure, but its value can reach units of kV at low gas pressures [23,24]. Such potential values can influence the formation of a beam plasma near a non-conducting target, which in turn will affect the processing of this target. In this connection, the aim of the present work was to investigate the peculiarities of beam plasma formation by means of an intense pulsed electron beam near a dielectric target in the forevacuum pressure range.

1. Experimental setup and research technique

A pulsed low-energy (up to 8 keV) electron beam of large radius was generated by a wide-aperture forevacuum plasma electron source, which was mounted on the flange of the vacuum chamber (Fig. 1). The parameters as well as a detailed description of the design and principle of operation of the electron source used are presented in [22]. The vacuum chamber was evacuated only by a mechanical forevacuum pump to the ultimate pressure level of 1 Pa. The operating pressure $p = 4-15$ Pa was controlled by the rate of gas (nitrogen) supply to the vacuum chamber, while the rate of chamber pumping by the forevacuum pump remained unchanged. High-purity nitrogen (nitrogen volume fraction of at least 99.99%) was used in the experiments. On the one hand, the choice of the working gas is due to the fact that nitrogen is one of the most common gases and is widely used in various beam, plasma and plasma chemical processes. On the other hand, nitrogen has an ionization cross-section which provides, as shown by studies with a continuous electron beam [26], a sufficiently dense beam plasma and, in the case of a forevacuum pulsed electron source, provides a higher operating pressure and/or longer beam pulse duration than gases with a larger ionization cross-section (e.g. argon) [22].

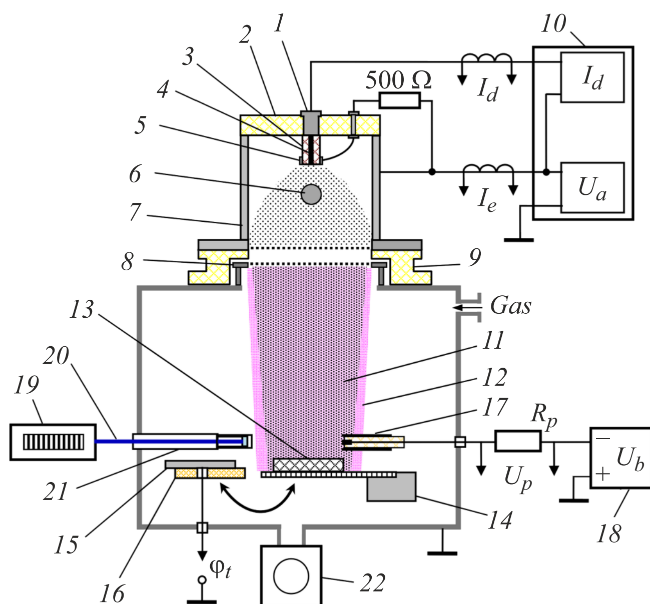

Figure 1. Schematic diagram of the experimental setup: *1* — current lead, *2* — insulator, *3* — ceramic insulator, *4* — cathode, *5* — trigger electrode, *6* — redistributing electrode, *7* — anode, *8* — accelerating electrode, *9* — high voltage insulator, *10* — power supply, *11* — electron beam, *12* — beam plasma, *13* — ceramic target, *14* — movement system, *15* — metal target, *16* — insulator, *17* — probe, *18* — dc voltage source, *19* — spectrometer, *20* — fiber optic, *21* — vacuum inlet, *22* — vacuum pump.

The electrical power supply unit of the plasma electron source provided a pulsed current I_d of the arc discharge forming the emission plasma at dc accelerating voltage U_a. Propagating in the vacuum chamber, the electron beam formed a beam plasma as a result of ionization of the working gas. A ceramic target made of alumina ceramic of VK 95-1 grade (dielectric constant — less than 10, specific bulk electrical resistivity — less than $10^{13}\,\Omega \cdot$cm) was installed on the electron beam propagation path. The receiving surface of the target had dimensions 50×50 mm, and the thickness of the target was 8 mm. The target was mounted on a movement system that allowed the target to move in the vacuum chamber. This made it possible to study the beam plasma formation both in the presence of a target and in case of „free" beam propagation. In both cases, a stainless steel collector was placed at the bottom of the vacuum chamber (at a distance of 45 cm from the electron beam source). During beam irradiation, the target was positioned so that its center coincided with the symmetry axis of the electron beam, the target plane was perpendicular to the beam propagation direction, and the distance from the electron source to the target was 25 cm. The diameter of the electron beam in the target area was 7 cm. To investigate the beam plasma formation during free propagation of the electron beam, the ceramic target was moved outside the beam propagating path. In a series of experiments, a stainless steel target, which was placed similarly to the ceramic target, was used to evaluate the magnitude of the potential arising on the ceramic target under electron beam irradiation and its effect on the formation of the beam plasma. The metal target had the same receiving surface 50×50 mm, but lower thickness — 2 mm. The stainless steel target was attached to a movement system via an insulator, allowing direct measurements of its floating potential φ_t when irradiated with a pulsed electron beam. This potential relative to ground was measured with a TESTEC HVP-15HF oscillographic probe (Fig. 1).

Since direct measurements of the electron beam current I_b during irradiation of a ceramic target are not possible, the beam current was estimated by measuring the current in the circuit of the high-voltage accelerating voltage source I_e, which is almost identical to the total emission current from the plasma. Our earlier studies have shown that the current I_b of the electron beam, as measured by the Faraday cup, is found to be smaller by 25–35% than the current I_e [22] as a function of pressure. The current I_e in the experiments was 10–40 A, the accelerating voltage U_a varied from 2 to 8 kV. The duration and pulse repetition rate of the discharge current and, consequently, of the electron beam current were 500 μs and 1 Hz, respectively. The beam parameters were chosen to provide an energy density in the pulse insufficient for appreciable vaporization of the target material. At the same time, the surfaces of the used targets were cleaned and subjected to prolonged beam irradiation before measurements of beam plasma parameters to remove the remaining fusible inclusions and absorbed gas.

The beam plasma density was measured using a single planar Langmuir probe with a protective shield preventing the electron beam from hitting the collecting surface of the probe. The plane of the collecting surface of the probe was parallel to the beam propagation direction (i.e. parallel to the beam symmetry axis), and in horizontal coordinates the position of the collecting surface of the probe coincided with the center of the target edge. The diameter of the collecting surface of the probe was 4 mm, and the stainless steel shield (guard ring) protruded 0.5 mm relative to the collecting surface of the probe. The probe was mounted on a movement system that allowed the distance L_p from the electron source and correspondingly the distance L_t from the target to the probe to be varied.

Since the electron energy distribution function in the beam plasma formed in nitrogen deviates markedly from the Maxwell distribution [6,28], the effective temperature of electrons was determined from the probe characteristic, as in the works [5,6]. Hereafter, the effective electron temperature, defined as two-thirds of the mean electron energy [6], will be referred to simply as the T_e electron temperature. Under experimental conditions, the electron temperature T_e ranged from 1.1 to 2 eV. The density n_i of the beam plasma was estimated from the saturation current I_i on the ion branch of the probe current-voltage characteristic by Bohm's formula [29,30] at a negative bias $U_b = -100$ V, at which saturation current I_i was always provided under experimental conditions. The current I_i in the planar probe circuit was determined by measuring the voltage U_p across the non-inductive resistor $R_p = 1400\,\Omega$, followed by conversion to current density j_i and plasma density n_i. Optical emission spectra of the beam plasma were measured with an Ocean Optics HR4000CG-UV-NIR spectrometer. An optical fiber placed in a special vacuum inlet with a quartz window was used to output optical radiation from the vacuum chamber. The input aperture of the optical fiber was oriented so that the symmetry axis of the optical fiber was directed to the beam symmetry axis and perpendicular to the beam propagation direction.

2. Experimental results

Fig. 2 shows typical oscillograms of the emission current I_e and ion current density j_i measured by the single Langmuir probe. Studies have shown that in the case of the ceramic target location on the electron beam propagation path, the ion current density j_i measured by the probe is higher (Fig. 2, curve *2*). Taking into account the insignificant change in the electron temperature T_e when the ceramic target is installed (with other parameters unchanged), the increase j_i indicates a corresponding increase in the density n_i of the beam plasma near the target compared to the density n_i at free beam propagation. The plots further show the densities (and normalized by the emission current I_e densities) of the beam plasma determined by taking into account the change in electron temperature. Increasing the emission current I_e leads to an increase in the electron temperature T_e and an almost linear increase in the density n_i of the plasma, with a stronger increase in the density n_i near the ceramic target (Fig. 3), i.e., the increment in the plasma density Δn_i, arising from the insertion of the target, grows with increasing I_e.

At an accelerating voltage of $U_a < 3$ kV, the emission current I_e and correspondingly the electron beam current I_b increase with increasing U_a, and at $U_a = 3$ kV, the current I_e reaches saturation [22]. Since at $U_a < 3$ kV it is not always possible to provide the same emission current as in the saturation mode, the discharge current I_d was kept constant during the study of the effect of the accelerating voltage on the beam plasma formation. For this reason, the values of the beam plasma density and the emission intensity of nitrogen spectral lines normalized to the emission current I_e

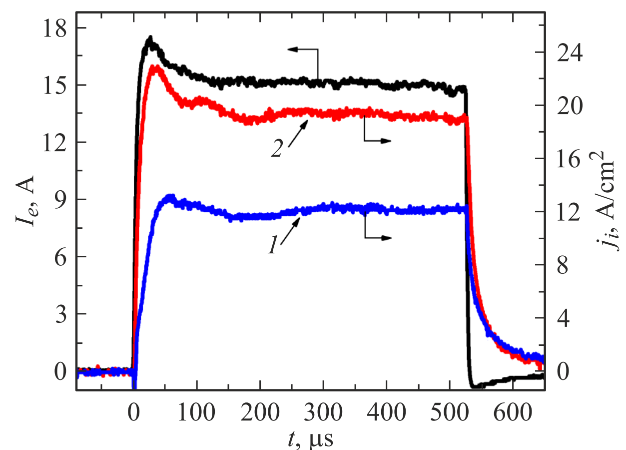

Figure 2. Oscillograms of emission current and ion current density measured by the probe at free electron beam propagation (*1*) and in the presence of a ceramic target on the beam path (*2*), $U_a = 6$ kV, $p = 8$ Pa.

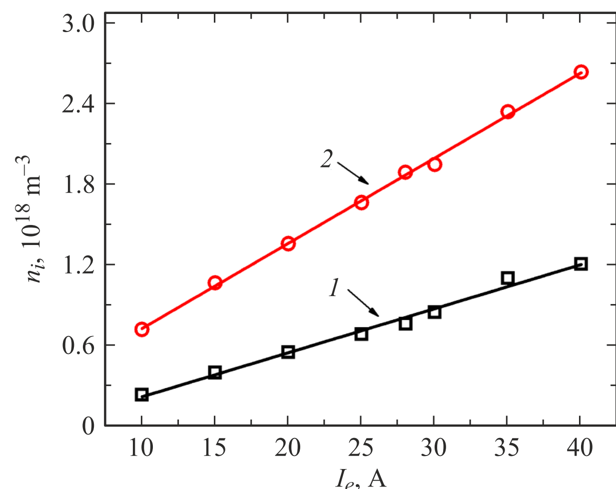

Figure 3. Dependence of beam plasma density n_i on emission current I_e at $L_p = 20$ cm, $p = 8$ Pa, $U_a = 7$ kV: *1* — free electron beam propagation; *2* — a ceramic target (probe-to-target distance $L_t = 5$ cm).

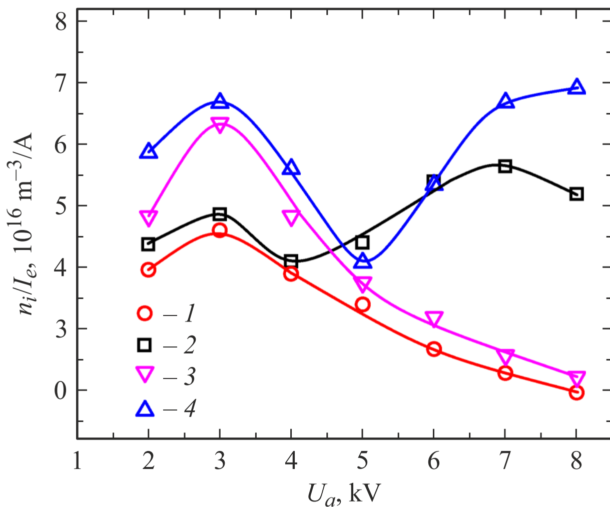

Figure 4. Dependence of the normalized beam plasma density n_i/I_e on the accelerating voltage U_a at different distance L_p at $p = 8$ Pa, in the saturation mode $I_e = 20$ A: *1, 2* — $L_p = 22$ cm ($L_t = 3$ cm); *3, 4* — $L_p = 20$ cm ($L_t = 5$ cm); *1, 3* — free propagation of the electron beam; *2, 4* – ceramic target is set.

(n_i/I_e and I_λ/I_e, respectively) are shown in Figs. 4,5. At a distance from the electron source $L_p < 15$ cm under the conditions of free electron beam propagation (i. e., without a target), the density n_i decreases monotonically with increasing accelerating voltage U_a over the entire pressure range investigated. At large distance ($L_p > 15$ cm), depending on the pressure of the working gas, the density n_i may depend non-monotonically on U_a. For example, at $L_p = 20$ cm and $p < 6$ Pa, the density of n_i decreases monotonically as U_a increases, and at $p = 6$ Pa and more, the density of n_i does not depend monotonically on U_a (Fig. 4, curve *1*). Initially, increasing the accelerating voltage U_a provides an increase in the density n_i of the beam plasma, but after the accelerating voltage reaches some threshold value U_{a-1} („threshold" voltage), further increase U_a leads to a decrease in the density n_i.

Near the ceramic target, the nature of the dependence of n_i on U_a appears to be more complicated. In addition to the presence of an extremum at the threshold voltage U_{a-1}, further 1–2 inflection points can be observed on the dependence of n_i on U_a (Fig. 4, curves *2, 4*). At $U_a > U_{a-1}$, (in the case of a „threshold" voltage U_{a-1} is reached), the plasma density n_i decreases as the accelerating voltage U_a increases, but when a certain „threshold" voltage U_{a-2} is reached, the plasma density n_i increases until a second threshold voltage U_{a-3} is reached. Then at $U_a > U_{a-3}$, the beam plasma density decreases again.

Studies of the optical emission spectra of the beam plasma confirmed that the beam plasma density is higher in the presence of the ceramic target, and also confirmed the complex nature of the dependence of the density n_i on the accelerating voltage. To investigate the beam plasma density near the target, the optical fiber input aperture was set at the same distance $L_p(L_t)$, as the single probe. Fig. 5 shows a typical emission spectrum of a beam plasma. The changes in the beam plasma density were estimated from the spectral line of the nitrogen molecular ion N_2^+ ($\lambda = 394.1$ nm), which belongs to the first negative system (FNS) of the nitrogen ion molecule radiation, and the spectral line of the nitrogen atomic ion N^+ ($\lambda = 661$ nm), which are quite commonly used to estimate the plasma density [6]. The intensities of the spectral lines $\lambda = 394.1$ nm (I_{394}) and $\lambda = 661$ nm (I_{661}) increase when the ceramic target is placed in the electron beam path. The dependences of the I_{394} and I_{661} intensities on U_a have a similar character to probe measurements of the dependence of n_i on U_a (Fig. 6). However, for the $\lambda = 394.1$ nm spectral line intensity of the nitrogen molecular ion I_{394}, the

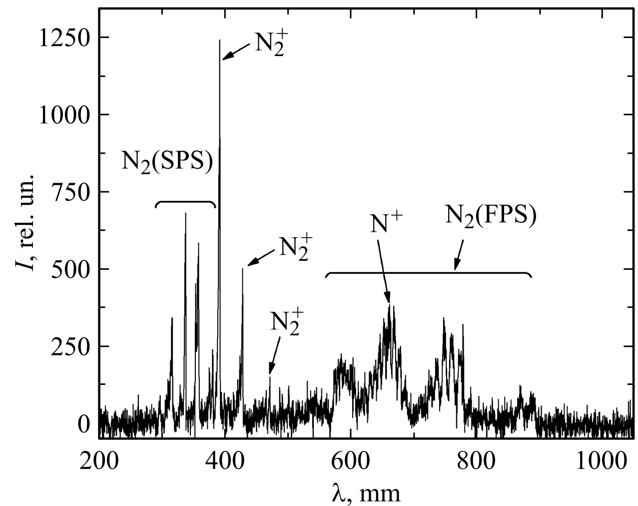

Figure 5. Typical emission spectrum of a beam plasma with a ceramic target installed in the electron beam path, $U_a = 4$ kV, $p = 9.6$ Pa (FPS and SPS — first and second positive emission systems of a neutral nitrogen molecule, respectively).

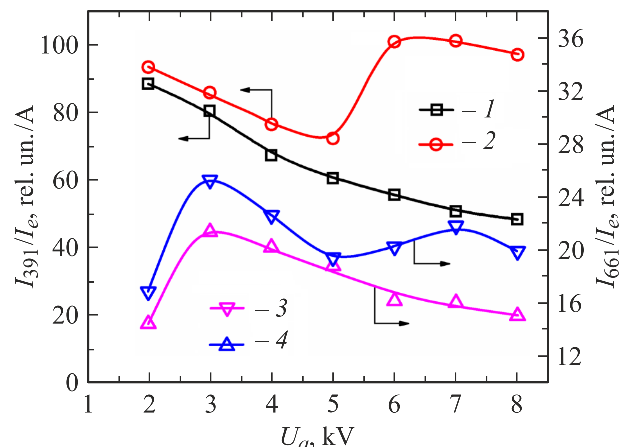

Figure 6. Dependences of normalized radiation intensities I_{394}/I_e and I_{661}/I_e on the accelerating voltage U_a, $p = 8$ Pa, $L_p = 22$ cm: *1, 3* — „free" electron beam propagation; *2, 4* — ceramic target is set.

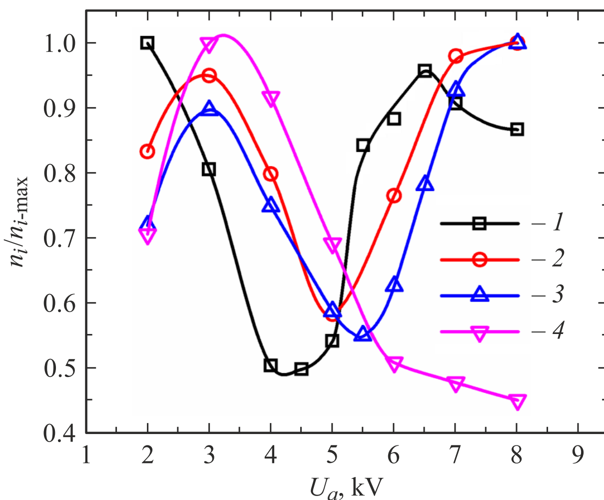

Figure 7. Dependence of relative beam plasma density $n_i/n_{i-\max}$ on accelerating voltage U_a at $L_p = 20$ cm; p: *1* — 5, *2* — 8, *3* — 9.6, *4* — 15 Pa.

threshold voltage $U_{\alpha-10}$ may not be observed. The observed differences seem to be related to the fact that the aperture of the optical fiber also receives radiation from upstream nitrogen ions, in particular, the intensity of radiation from these ions can be higher at low accelerating voltage. In addition, the emission spectrum of the beam plasma also shows the spectra of the first positive system (FPS) of the neutral nitrogen molecule radiation [6,31], whose spectral lines on the wavelength scale lie close to the spectral line $\lambda = 661$ nm under consideration. This leads to the fact that due to insufficiently high resolution of the spectrometer used, the intensity of the spectral line and $\lambda = 661$ nm (I_{661}) may be distorted due to overlapping of neighboring spectral bands. Therefore, the spectrometer used does not allow us to determine the exact (real) values of the beam plasma density, but it allows us to monitor the trends in the plasma density.

An increase in gas pressure leads to an increase in the values of voltages U_{a-2} and U_{a-3}. Therefore, U_{a-2} and U_{a-3} extrema may not be observed when some pressure is reached (Fig. 7). For example, at $L_p = 22$ cm, when the pressure $p = 15$ Pa is reached, the values of voltages U_{a-2} and U_{a-3} exceed 8 kV, resulting in only a monotonic decrease in plasma density after the boundary voltage U_{a-1}. At the same time, under these conditions, the beam plasma density near the target remains higher than in the case of free electron beam propagation. The difference Δn_i between the plasma density with and without the target decreases as the gas pressure increases. The density n_i of the beam plasma can be varied by varying the emission current I_e of the electron beam, the accelerating voltage U_a and the gas pressure p. The obtained densities n_i are comparable to the beam plasma densities obtained, for example, in works [4,12].

3. Discussion of results

Since the fraction of residual atmosphere molecules (H_2, O_2, vapors H_2O and etc.) is small compared to the working gas N_2, the contribution of these molecules to the formation of the beam plasma is neglected. There is a rather detailed beam plasma model [6], which considers various processes during plasma formation by means of a low-energy electron beam in a nitrogen atmosphere in a similar pressure range. In the present work, we shall limit ourselves to the consideration of the processes associated with the formation of nitrogen ions. A significant contribution to the formation of nitrogen ions can be made by the stepwise ionization of the nitrogen molecule in the metastable state $A_3\Sigma_u^+$ [32]. However, according to the estimates made in [6], at the pressures considered, the electron beam forms relatively few metastable nitrogen molecules in the state $A_3\Sigma_u^+$, so the contribution of these molecules will be neglected. The cross sections of the processes of formation of molecular nitrogen ions N_2^+, excited molecular ions $N_2^+(B^2\Sigma_u^+)$ and atomic ions N^+, as well as the process of dissociation of nitrogen molecule by electron impact, which make the greatest contribution to the formation of the beam plasma [6], are presented in the table. The table shows that the value of the cross section of the process of formation of molecular nitrogen ion N_2^+ $(e + N_2 \rightarrow N_2^+ + 2e)$ is times larger than the cross sections of the processes $e + N_2 \rightarrow N_2^+(B^2\Sigma_u^+) + 2e$ and $e + N_2 \rightarrow N^+ + N + 2e$. The cross section of the $e + N \rightarrow N^+ + 2e$ process appears to be smaller by a factor of 1.65−1.35 fold compared to the $e + N_2 \rightarrow N_2^+ + 2e$ process, but the dissociation of the nitrogen molecule $e + N_2 \rightarrow N + N + e$ must first occur for its realization. The cross section of the dissociation process of the nitrogen molecule decreases significantly with increasing energy E_e of electrons and at $E_e \geq 0.5$ keV is more than 5 times smaller than the cross section of the process $e + N_2 \rightarrow N_2^+ + 2e$. Therefore, further for simplicity, we consider the formation of only molecular nitrogen ions N_2^+. The cross section of the $e + N_2 \rightarrow N_2^+ + 2e$ process will hereafter be referred to simply as the ionization cross section σ_i of gas.

The differences in beam plasma formation qualitatively observed in the experiment in the presence of a ceramic target and in the case of free electron beam propagation can be explained as follows. Since the beam collector is located at a considerable distance from the planar probe (45 cm), without the ceramic target, beam plasma formation in „free" space at the considered distances $L_p = 20{-}22$ cm is provided due to gas ionization by accelerated beam electrons as well as by fast (from the „tail" of the electron energy distribution) electrons of the beam plasma. According to the estimates made in the works [6,38], the rate of gas ionization by fast plasma electrons is much smaller than the rate of ionization by accelerated beam electrons. Therefore, the contribution of plasma electrons to the beam plasma formation can be neglected. In approximation of

Cross sections (in m^2) of the formation of molecular ions N_2^+, excited molecular ions $N_2^+(B^2\Sigma_u^+)$, atomic ions N^+, and of the dissociation process of a nitrogen molecule when interacting with electrons for different electron energies E_e

Process	$E_e = 0.1$ keV	$E_e = 0.5$ keV	$E_e = 2$ keV	$E_e = 4$ keV	Ref.
$e + N_2 \to N_2^+ + 2e$	$2.615 \cdot 10^{-20}$	$1.428 \cdot 10^{-20}$	$0.521 \cdot 10^{-20}$	$0.25 \cdot 10^{-20}$	[33]
$e + N_2 \to N_2^+(B^2\Sigma_u^+) + 2e$	$0.232 \cdot 10^{-20}$	$0.13 \cdot 10^{-20}$	$0.05 \cdot 10^{-20}$	$0.03 \cdot 10^{-20}$	[34]
$e + N_2 \to N^+ + N + 2e$	$0.65 \cdot 10^{-20}$	$0.3 \cdot 10^{-20}$	$0.01 \cdot 10^{-20}$	$< 0.009 \cdot 10^{-20}$	[35]
$e + N_2 \to N + N + e$	$1.9 \cdot 10^{-20}$	$0.3 \cdot 10^{-20}$	$0.09 \cdot 10^{-20}$	$0.04 \cdot 10^{-20}$	[36]
$e + N \to N^+ + 2e$	$1.58 \cdot 10^{-20}$	$0.8 \cdot 10^{-20}$	$0.29 \cdot 10^{-20}$	$0.18 \cdot 10^{-20}$	[37]

the homogeneous distribution of the current density j_e and, accordingly, the flux density of accelerated electrons n_b over the electron beam cross section, we can write down the balance equation for ions, assuming that the loss of ions occurs mainly due to the Bohm current from the plasma boundary:

$$0.4 n_i \sqrt{\frac{2kT_e}{M_i}} \frac{S_p}{n_g} = n_b \sigma_i(U_a) \sqrt{\frac{2eU_a}{m_e}} L_p S_b, \qquad (1)$$

where k — the Boltzmann constant, M_i — the mass of the ion, n_g — the density of gas neutrals determined by gas pressure p, S_p — the area of the plasma from which the beam plasma loses ions, e — the elementary charge, m_e — electron mass, L_p — length of the cylindrical area occupied by the beam plasma, S_b — the cross-sectional area of the beam, $\sigma_i(U_a)$ — ionization cross section of gas by accelerated beam electrons.

The dependence of the ionization cross section $\sigma_i(U_a)$ on the accelerating voltage (electron energy E_e) can be estimated using the formulas presented in [33]. At the accelerating voltage U_a used, the electron energy of the beam E_e corresponds to a decreasing branch of the dependence of the ionization cross section σ_i on the energy E_e, and when increasing E_e from 2 to 8 keV, the ionization cross section σ_i of nitrogen decreases by about 2.2 fold [33]. Therefore, the observed decrease in density n_i can be attributed to a decrease σ_i by an increase U_a. A decrease in the density n_i of the beam plasma with increasing accelerating voltage U_a (beam electron energy E_e) was also observed when the beam plasma was formed by a continuous electron beam [25]. In addition, as U_a increases, the scattering of the electron beam on the working gas molecules decreases, and the beam becomes more „focused", which may also contribute to the formation of the beam plasma at the beam periphery where the probe is located. The non-monotonic dependence n_i on U_a observed at $L_p > 15$ cm is apparently due to a change in the number of electrons, i.e., density of the accelerated electrons flux n_b, which at the distance under consideration have an energy E_e sufficient to ionize the gas. The decrease in electron density n_b and energy loss by the beam electrons as the beam propagates through the gas are due to scattering of electrons on gas molecules and reactions of ionization, excitation, dissociation of molecules and atoms of the working gas (the cross sections of these reactions increase with decreasing U_a [33–37]). At $U_a < U_{a-1}$ at distances $L_p > 15$ cm, an increase in the accelerating voltage provides an increase in the density of accelerated electrons n_b, possessing energy E_e, sufficient to ionize the gas at the distance under consideration L_p (i.e. the number of ionization acts of gas molecules increases). At $U_a > U_{a-1}$, the number of electrons with sufficient energy for ionization E_e changes weakly (or practically does not change) as the accelerating voltage increases further, and the decrease in the ionization cross section σ_i plays a decisive role.

After cleaning and pre-irradiation (degassing) of the ceramic target, the composition of optical radiation does not differ from the case of beam plasma formation at free electron beam propagation. For this reason, we assume that the composition of the gas atmosphere near the target is practically the same as in the case of free beam propagation. When a ceramic target is irradiated with an electron beam, electron-induced secondary electron emission occurs from the target surface. Also, since a negative potential occurs on the surface of the ceramic target irradiated by the electron beam, ions from the beam plasma, accelerated by the potential difference U_t between the beam plasma and the ceramic target, cause ion-electron emission when bombarding the target. The electron yield factor γ_e of the electron-induced secondary electron emission depends non-monotonically on the electron energy [39], while the yield factor γ_i of the ion-electron emission increases as the ion energy [40] increases. The potential difference U_t can be estimated, as

$$U_t = \varphi_p - \varphi_t, \qquad (2)$$

where φ_t — the potential of the ceramic target surface relative to the grounded chamber walls, φ_p — the potential of the beam plasma. The potential of the beam plasma φ_p with respect to the vacuum chamber walls can be estimated by the formula [30]:

$$\varphi_p = -\ln\left(0.4\sqrt{\frac{\pi m_e}{4M_i}}\right)\frac{kT_e}{e}. \qquad (3)$$

For the electron beam parameters used, at voltages U_{a-2} and U_{a-3}, the surface potential of the ceramic target is

much larger than the beam plasma potential, so we can assume $U_t \approx \varphi_t$.

Electrons emitted from the surface of the ceramic target and accelerated by the potential difference U_t, with sufficient energy, also ionize the working gas, which provides an additional increase in the beam plasma density near the target. Taking into account the emission of electrons from the ceramic surface, we can write down balance equations for the currents on the target and the ion balance similar to those obtained in the work [25] when irradiating an isolated metallic target with a continuous electron beam:

$$\left(1-\gamma_e(U_{at})\right) j_e S_t + n_i e\sqrt{\frac{8kT_e}{\pi m_e}}\exp\left[-\frac{eU_t}{kT_e}\right]S_t - \left(1+\gamma_i(U_t)\right)0.4 n_i e\sqrt{\frac{2kT_e}{M_i}}S_t = 0, \quad (4)$$

$$0.4n_i\sqrt{\frac{2kT_e}{M_i}}\frac{S_p}{n_g} = n_b\sigma_i(U_a)\sqrt{\frac{2eU_a}{m_e}}L_pS_b + \left(\gamma_e(U_{at})j_e + \gamma_i(U_t)0.4en_i\sqrt{\frac{2kT_e}{M_i}}\right) \times \frac{\sigma_i(U_t)}{e}\left(\frac{U_t}{W_i}\right)\left(1-\exp\left[-L_pn_g\sigma_i(U_t)\right]\right)L_pS_t, \quad (5)$$

where j_e — the beam current density, which can be estimated as $\beta I_e/S_b$, $\beta = 0.65{-}0.75$ (depending on the pressure p), W_i — the ion-electron pair formation energy, $\gamma_e(U_{at})$ — electron-induced secondary electron emission coefficient depending on U_a and U_t ($U_{at} = U_a - U_t$), $\gamma_t(U_t)$ — ion-electron emission coefficient depending on U_t. The dependence of the ionization cross section $\sigma_i(U_t)$ on the potential difference U_t can also be estimated from the formulas presented in [33].

In expression (4), the first term represents the flux of beam electrons onto the target minus the flux of secondary electrons emitted from the target surface under the action of the beam electrons. The second term describes the contribution of the flux of thermal electrons from the beam plasma through the potential barrier U_t onto the target. The third term describes the Bohm current of ions from the beam plasma, which compensates for the negative charge on the target surface, and the electron flux that occurs when the target is bombarded by ions accelerated by the potential difference U_t. In (5), the loss of ions due to their departure from the beam plasma surface (left part) is compensated by ion generation due to the impact ionization of gas by beam electrons (first term of the right part) and ionization of gas by electrons emitted from the ceramic surface and accelerated by the potential difference U_t along the direction from the target (second term of the right part). The multiplier $\left(1-\exp\left[-L_pn_g\sigma_i(U_t)\right]\right)$ of the right-hand side of formula (5) is responsible for the decrease in gas ionization efficiency with increasing secondary electron energy when the secondary electron energy exceeds 100 eV [33].

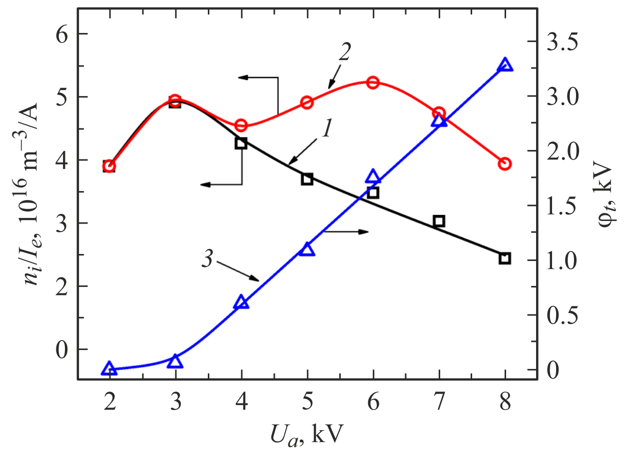

Figure 8. Dependences of normalized beam plasma density n_i/I_e and potential φ_t on accelerating voltage U_a at $p = 8$ Pa: *1* — n_i/I_e at grounded target; *2* — n_i/I_e at isolated metal target; *3* — φ_t potential of the isolated target.

When irradiating isolated and nonconducting targets with a continuous electron beam with currents up to hundred mA, the absolute value of the negative potential of the target does not exceed hundreds of volts [23]. Therefore, in [25,41], the coefficient of electron-induced secondary electron emission γ_e depended only on the accelerating voltage, and the ion-electron emission made a small contribution, and was neglected in paper [41]. However, when irradiated with an intense pulsed electron beam (with currents greater than 1 A), the negative potential can reach units of keV [24]. Therefore, due to possible significant inhibition of the beam electrons by the potential difference U_t in expressions (4) and (5), the coefficient of electron-induced secondary electron emission $\gamma_e(U_{at})$ may depend significantly on U_a and U_t ($U_{at} = U_a - U_t$). The coefficient $\gamma_e(U_t)$ increases with increasing ion energy, so the ion-electron emission contribution grows as the U_t increases. Increasing the emission current (beam current) at a constant accelerating voltage leads to a greater increase in the plasma density near the target due to an increase in the number of electrons emitted from the target surface and accelerated by the potential difference U_t. The magnitude of the negative potential φ_t on the nonconducting target and, accordingly, the potential difference U_t decreases in modulus with increasing working gas pressure and increases with increasing accelerating voltage and electron beam current [23,24]. Therefore, the observed complex character of the dependence of n_i on U_a is due to the change in the negative potential at the surface of the ceramic target. The relationship between the non-monotonic dependence of n_i on U_a and the target potential φ_t is confirmed by a model experiment with a metallic target irradiated by an electron beam. At the grounded metal target, the dependence of the beam plasma density n_i on the accelerating voltage U_a has the same character as at „free" electron beam propagation (Fig. 8, curve *1*). However, in the case of the isolated

metallic target, as the U_a increases, an increase in the φ_t potential is observed, and a non-monotonic dependence of n_i on U_a appears (Fig. 8, curve *2*), similar to the same dependence for the ceramic target. Optical measurements showed that the intensity of spectral lines at the grounded metallic target is slightly higher than at „free" electron beam propagation, but no inflection points corresponding to voltages U_{a-2} and U_{a-3} are observed in the dependences of spectral line intensities on the accelerating voltage. For the isolated metallic target, the dependencies of I_{394}/I_e and I_{661}/I_e on U_a have a complex character similar to those for the ceramic target. The quantitative differences in the dependences for the isolated metallic target and the ceramic target are due to the different electrophysical properties of the targets. In particular, for example, the magnitude of the potential to which the surface of the ceramic target is charged depends on the dielectric constant of the material [42].

At the acceleration voltages used, the electron yield from the surface of alumina ceramic [39] and stainless steel [43] decreases with increasing U_a. However, an increase of U_t leads to electron deceleration and an increase in the secondary emission coefficient $\gamma_e(U_{at})$. The increase of U_t also leads to an increase in the ion-electron emission coefficient $\gamma_i(U_t)$. Therefore, at first (at $U_a > U_{a-2}$) with increasing U_a, there is an increase in the density n_i of the beam plasma due to an increase in the number of electrons emitted from the target surface and accelerated by the potential difference U_t. Then, when the accelerating voltage exceeds the value of U_{a-3}, despite the increase of $\gamma_i(U_t)$, further increase of the potential difference U_t leads to a decrease of the gas ionization cross section $\sigma_i(U_t)$, which together with the decrease of the gas ionization cross section by beam electrons $\sigma_i(U_a)$, leads to a decrease of n_i. The shift of the U_{a-2} and U_{a-3} voltages toward higher values with increasing gas pressure is due to the compensation of the negative charge on the surface of the ceramic target and the corresponding decrease of U_t.

Conclusion

The processes of beam plasma formation near a dielectric target made of alumina ceramics under irradiation by an intense pulsed electron beam with a current of tens of amperes in the forevacuum pressure range (4−15 Pa) have been investigated. It is shown that the beam plasma density near the irradiated ceramic target is higher than at „free" electron beam propagation. The plasma density increment resulting from the ceramic target installation depends on the emission current (beam current), gas pressure, and accelerating voltage. In addition, the beam plasma density near the target depends non-monotonically on the accelerating voltage. The observed dependences for the beam plasma density near the target are due to the emission of electrons from the target surface and the uncompensated negative potential arising due to the electron beam irradiation. This potential creates an electric field that inhibits the beam electrons and accelerates the electrons emitted from the ceramic surface. The influence of the negative potential is confirmed by the fact that an increase in gas pressure, which provides a modulo decrease in the negative potential, leads to a smaller increment in the beam plasma density when the ceramic target is installed. By varying the electron beam current and accelerating voltage, the beam plasma density can be controlled.

Funding

The research is performed under the grant support of the Ministry of Science and Higher Education of the Russian Federation №FEWM-2023-0012.

Conflict of interest

The authors declare that they have no conflict of interest.

References

[1] P.K. Chu, X.P. Lu. *Low Temperature Plasma Technology: Methods and Applications* (CRC Press, Boca Raton, 2013)
[2] E.B. Hooper Jr, O.A. Anderson, P.A. Willmann. Phys. Fluids, **22** (12), 2334 (1979). DOI: 10.1063/1.862545
[3] K.S. Klopovsky, A.V. Mukhovatova, A.M. Popov, N.A. Popov, O.B. Popovicheva, T.V. Rakhimova. J. Phys. D: Appl. Phys., **27** (7), 1399 (1994). DOI: 10.1088/0022-3727/27/7/010
[4] S.G. Walton, C. Muratore, D. Leonhardt, R.F. Fernsler, D.D. Blackwell, R.A. Meger. Surf. Coatings Technol., **186** (1−2), 40 (2004). DOI: 10.1016/j.surfcoat.2004.04.007
[5] E.H. Lock, R.F. Fernsler, S.G. Walton. Plasma Sources Sci. Technol., **17** (2), 025009 (2008). DOI: 10.1088/0963-0252/17/2/025009
[6] E.H. Lock, R.F. Fernsler, S.P. Slinker, I.L. Singer, S.G. Walton. J. Phys. D: Appl. Phys., **47**, 425206 (2014). DOI: 10.1088/0022-3727/47/42/425206
[7] J.A. Aguilera, C. Aragon. Spectrochim. Acta Part B: Atomic Spectroscopy, **59** (12), 1861 (2004). DOI: 10.1016/j.sab.2004.08.003
[8] L.J. Radziemski. *Lasers-Induced Plasmas and Applications* (CRC Press, Boca Raton, 2020)
[9] T. Vasilieva, S. Lopatin, V. Varlamov, V. Miasnikov, A.M. Hein, M. Vasiliev. Pure Appl. Chem., **88** (9), 873 (2016). DOI: 10.1515/pac-2016-0603
[10] T.M. Vasilieva, I.K. Naumova, O.V. Galkina, E.V. Udoratina, L.A. Kuvschinova, M.N. Vasiliev, Khin Maung Htay, Htet Ko Ko Zaw. IEEE Transactions on Plasma Sci., **48** (4), 1035 (2020). DOI: 10.1109/TPS.2020.2980200
[11] A.S. Klimov, I.Yu. Bakeev, E.M. Oks, V.T. Tran, A.A. Zenin. Vacuum, **196**, 110722 (2022). DOI: 10.1016/j.vacuum.2021.110722
[12] D. Leonhardt, C. Muratore, S.G. Walton, D.D. Blackwell, R.F. Fernsler, R.A. Meger. Surf. Coatings Technol., **177**, 682 (2004). DOI: 10.1016/j.surfcoat.2003.08.007
[13] S.G. Walton, D.R. Boris, S.C. Hernandez, E.H. Lock, T.B. Petrova, G.M. Petrov, E.A. Joseph. Microelectron. Engineer., **168**, 89 (2017). DOI: 10.1016/j.mee.2016.11.003

[14] N.V. Gavrilov, A.I. Men'shakov. Tech. Phys., **57** (3), 399 (2012). DOI: 10.1134/S1063784212030073
[15] T. Vasilieva, I. Sokolov, A. Sigarev, A. Tun Win. Open Chem., **13** (1), 204 (2015). DOI: 10.1515/chem-2015-0015
[16] S. Ghosh, D.R. Boris, S.C. Hernandez, C.A. Zorman, S.G. Walton, R.M. Sankaran. Plasma Processes and Polymers, **14** (12), 1700079 (2017). DOI: 10.1002/ppap.201700079
[17] V.O. Konstantinov, V.G. Shchukin, R.G. Sharafutdinov, V.M. Karsten, G.G. Gartvich, O.I. Semenova. Plasma Phys. Reports, **36**, 1278 (2010). DOI: 10.1134/S1063780X10130313
[18] R.G. Sharafutdinov, V.O. Konstantinov, V.I. Fedoseev, V.G. Shchukin. Plasma Phys. Reports, **44**, 886 (2018). DOI: 10.1134/S1063780X18090143
[19] R. Nishio, K. Tuchida, M. Tooma, K. Suzuki. J. Appl. Phys., **72** (10), 4548 (1992). DOI: 10.1063/1.352334
[20] A.A. Zenin, A.S. Klimov, V.A. Burdovitsin, E.M. Oks. Tech. Phys. Lett., **39** (5), 454 (2013). DOI: 10.1134/S1063785013050271
[21] V.A. Burdovitsin, I.Yu. Bakeev, A.A. Zenin, D.B. Zolotukhin, A.V. Kazakov, A.S. Klimov, A.V. Medovnik, E.M. Oks, A.V. Tyunkov. Dokladi TUSUR, **19** (2), 5 (2016). (In Russian). DOI: 10.21293/1818-0442-2016-19-2-5-10
[22] A.V. Kazakov, A.V. Medovnik, E.M. Oks, N.A. Panchenko. Rev. Sci. Instruments, **91**, 093304 (2020). DOI: 10.1063/5.0023172
[23] V.A. Burdovitsin, A.S. Klimov, A.V. Medovnik, E.M. Oks. Plasma Sources Sci. Technol., **19** (5), 055003 (2010). DOI: 10.1088/0963-0252/19/5/055003
[24] V.A. Burdovitsin, V.S. Gul'kina, A.V. Medovnik, E.M. Oks. Tech. Phys., **58** (12), 1837 (2013). DOI: 10.1134/S1063784213120086
[25] V.A. Burdovitsin, E.M. Oks, D.B. Zolotukhin. J. Phys. D: Appl. Phys., **51** (30), 304006 (2018). DOI: 10.1088/1361-6463/aace4a
[26] A.S. Klimov, E.M. Oks, A.P. Andreichik, M.I. Lomaev. Tech. Phys., **62** (2), 218 (2017). DOI: 10.1134/S1063784217020128
[27] D.B. Zolotukhin, V.A. Burdovitsin, E.M. Oks. Plasma Sources Sci. Technol., **25** (2), 015001 (2015). DOI: 10.1088/0963-0252/25/1/015001
[28] V.P. Konovalov, M.A. Skorik, E.E. Son. *Proceedings of XX International Conference on Phenomena in Ionized Gases* (Italy, 1991), p. 405–406.
[29] O.V. Kozlov. *Electrical Probe in Plasma* (Atomizdat, M., 1969) (in Russian).
[30] Yu.P. Raizer. *Gas Discharge Physics* (Springer, Berlin, 1991).
[31] R.S. Mangina, J.M. Ajello, R.A. West, D. Dziczek. Astrophys. J. Supplement Series, **196** (1), 13 (2011). DOI: 10.1088/0067-0049/196/1/13
[32] V. Guerra, P.A. Sa, J. Loureiro. Europ. Phys. J.—Appl. Phys., **28**, 125 (2004). DOI: 10.1051/epjap:2004188
[33] W. Hwang, Y.K. Kim, M.E. Rudd. J. Chem. Phys., **104**, 2956 (1996). DOI: 10.1063/1.471116
[34] D.E. Shemansky, X. Liu. J. Geophys. Research: Space Phys., **110** (A7), A073071 (2005). DOI: 10.1029/2005JA011062
[35] Y. Itikawa. J. Phys. Chem. Refer. Data, **35**, 31 (2006). DOI: 10.1063/1.1937426
[36] S.G. Walton, D.R. Boris, S.C. Hernández, E.H. Lock, Tz.B. Petrova, G.M. Petrov, R.F. Fernsler. ECS J. Solid State Sci. Technol., **4** (6) N5033 (2015). DOI: 10.1149/2.0071506jss
[37] Y.-K. Kim, J.-P. Desclaux. Phys. Rev. A, **66**, 012708 (2002). DOI: 10.1103/PhysRevA.66.012708
[38] A.V. Tyunkov, A.A. Andronov, Y.G. Yushkov, D.B. Zolotukhin. Pisma v ZHTF, **49** (10), 13 (2023) (in Russian). DOI: 10.21883/PJTF.2023.10.55427.19539
[39] J. Cazaux. Nucl. Instruments and Methods in Phys. Res. Section B: Beam Interactions with Materials and Atoms, **244** (2), 307 (2006). DOI: 10.1016/j.nimb.2005.10.006
[40] N.R. Rajopadhye, V.A. Joglekar, V.N. Bhoraskar, S.V. Bhoraskar. Solid State Commun., **60** (8), 675 (1986). DOI: 10.1016/0038-1098(86)90266-8
[41] V.A. Burdovitsin, D.B. Zolotukhin, E.M. Oks, N.A. Panchenko. J. Phys. D: Appl. Phys., **52** (28), 285204 (2019). DOI: 10.1088/1361-6463/ab1381
[42] E.I. Rau, E.N. Evstaf'eva, M.V. Andrianov. Phys. Solid State, **50**, 621 (2008). DOI: 10.1134/S1063783408040057
[43] M. Kaminsky. *Atomic and Ionic Impact Phenomena on Metal Surfaces* (Academic, NY., 1965)

Translated by Y.Deineka